Journal of
Instrumentation

The FAMU experiment at RIKEN-RAL for high-precision HFS muon spectroscopy

To cite this article: M. Bonesini *et al* 2026 *JINST* **21** C01029

Published by IOP Publishing for Sissa Medialab

Received: *November 30, 2025*
Accepted: *January 1, 2026*
Published: *January 22, 2026*

17[TH] Topical Seminar on Innovative Particle and Radiation Detectors
Siena, Italy
15–19 September 2025

The FAMU experiment at RIKEN-RAL for high-precision HFS muon spectroscopy

M. Bonesini,[a,1,*] R. Benocci,[a,1] A. Adamczak,[b] D. Bakalov,[c] G. Baldazzi,[d] M. Baruzzo,[e] R. Bertoni,[a] S. Capra,[f] D. Cirrincione,[e] M. Clemenza,[a] L. Colace,[g] M. Danailov,[e,2] P. Danev,[c] A. de Bari,[h] C. De Vecchi,[h] D. Di Ferdinando,[d] E. Fasci,[i] R. Gaigher,[a] L. Gianfrani,[i] A.D. Hillier,[j] K. Ishida,[k] J.S. Lord,[j] A. Menegolli,[h] E. Mocchiutti,[e] S. Monzani,[e,l] L. Moretti,[i] G. Morgante,[d,3] C. Pizzolotto,[e] A. Pullia,[f] M. Pullia,[h,4] R. Ramponi,[f,m] H.E. Roman,[a] M. Rossella,[h] R. Rossini,[h] A. Sbrizzi,[d] M. Stoilov,[c] J.J. Suárez-Vargas,[e] G. Toci,[n] L. Tortora,[g] E. Vallazza,[a] K. Yokoyama[j] and A. Vacchi[e,k,l]

[a] *Sezione INFN, Dipartimenti di Fisica e di Scienze Ambientali e della Terra, Università di Milano Bicocca, Piazza Scienza 3, Milano, Italy*
[b] *Institute of Nuclear Physics, Polish Academy of Sciences, Radzikowskiego 152, Kraków, Poland*
[c] *INRNE, Bulgarian Academy of Sciences, blvd. Tsaridgradsko ch 72, Sofia, Bulgaria*
[d] *Sezione INFN and Dipartimento di Fisica ed Astronomia "A. Righi", Università di Bologna, viale Berti Pichat 6/2, Bologna, Italy*
[e] *Sezione INFN di Trieste, via A. Valerio 2, Trieste, Italy*
[f] *Sezione INFN di Milano and Dipartimento di Fisica, Università degli Studi, via Celoria 16, Milano, Italy*
[g] *Sezione INFN and Dipartimento di Ingegneria, Università di Roma Tre, via della Vasca Navale 84, Roma, Italy*
[h] *Sezione INFN and Dipartimento di Fisica "A. Volta", Università di Pavia, via A. Bassi 6, Pavia, Italy*
[i] *Sezione INFN di Napoli and Dipartimento di Fisica, Università della Campania "L. Vanvitelli", viale Lincoln 5, Caserta, Italy*
[j] *ISIS Neutron, Muon Source, STFC Rutherford-Appleton Laboratory, Didcot, U.K.*
[k] *Riken Nishina Center, RIKEN, 2-1 Hirosawa, Wako, Saitama, Japan*
[l] *Dipartimento di Scienze Matematiche, Informatiche e Fisiche, Università di Udine, via delle Scienze 206, Udine, Italy*
[m] *IFN-CNR and Dipartimento di Fisica, Politecnico di Milano, Piazza Leonardo da Vinci 32, Milano, Italy*
[n] *INO-CNR, via Madonna del Piano 10, Sesto Fiorentino, Italy*

E-mail: maurizio.bonesini@unimib.it

[*] Corresponding author.
[1] Speaker.
[2] Sincrotrone Elettra Trieste, Basovizza, Italy
[3] INAF-OAS Bologna, Bologna, Italy
[4] Centro Nazionale di Adroterapia Oncologica (CNAO), Pavia, Italy

https://doi.org/10.1088/1748-0221/21/01/C01029

2026 JINST 21 C01029

Abstract: The FAMU experiment at RIKEN-RAL aims to measure with high precision the ground state hyperfine splitting (1S HFS) of muonic hydrogen and thus determine the proton Zemach radius. A novel method based on the detection of X-rays emitted by μO after the muon transfer from μH to oxygen is used. A high performance X-ray detectors' system and an innovative mid-infrared (MIR) laser system were therefore developed. The X-ray detector's system is mainly based on $LaBr_3$:Ce crystals read by SiPM arrays. From the MIR laser frequency value, known with precision < 10^{-5}, the energy of the HFS transition may be accurately measured, as $\Delta E_{\mathrm{HFS}} = h\nu_{\mathrm{HFS}}$.

Keywords: Gamma detectors (scintillators, CZT, HPGe, HgI etc); Muon spectrometers

2026 JINST 21 C01029

Contents

1 Introduction

As the Bohr radius scales inversely with the orbiting particle's mass, the radius of a muonic atom is about 1/200 that of the corresponding electronic one. This drastic reduction in size causes the muon's wavefunction to overlap significantly with the nuclear volume, especially for high atomic numbers (Z). Consequently, the X-ray transition energies in muonic atoms are strongly influenced by the nuclear charge distribution, allowing accurate determinations of nuclear radii and providing stringent tests of QED in strong electromagnetic fields [1].

High-precision measurements of muonic atomic transition lines attracted renewed attention following the unexpected results of the Lamb shift measurement in muonic hydrogen (μ-p) [2, 3], which enabled a precise determination of the proton charge radius. This value was inconsistent with earlier results obtained through alternative experimental methods [1]. Because the energy spectrum of muonic hydrogen is more sensitive to the proton's internal structure than that of ordinary hydrogen, this breakthrough in laser spectroscopy demonstrated the remarkable diagnostic power of the μ-p system. The discrepancy uncovered by this experiment became known as the "proton radius puzzle" and initiated a decade of intensive theoretical and experimental efforts, emphasizing the need to continue investigations of the muonic hydrogen atom.

Motivated by this development, earlier proposals to determine the ground-state hyperfine splitting (HFS) in muonic hydrogen using laser spectroscopy were revived [4].

The ground-state hyperfine splitting (HFS) in muonic hydrogen is given by:

$$\Delta E^{\mathrm{hfs}}_{1s} = E_F \left(1 + \delta_{\mathrm{QED}} + \delta_{\mathrm{str}} + \delta_{\mathrm{pol}}\right), \tag{1.1}$$

where E_F is the Fermi energy, representing the dominant magnetic dipole-dipole interaction term. The correction terms $\delta_{\mathrm{QED}}, \delta_{\mathrm{str}}$ and δ_{pol} account respectively for higher-order QED effects, proton finite-size (structure) contributions and nuclear polarizability effects.

The hyperfine splitting is particularly sensitive to the proton's magnetic structure, encapsulated in the *Zemach radius* R_Z [5], defined as

$$R_Z = \int d^3r\, r \,\frac{\rho_E(r)\,\rho_M(r)}{\int d^3r\, \rho_E(r) \int d^3r\, \rho_M(r)}, \tag{1.2}$$

where $\rho_E(r)$ is the proton's electric charge density, $\rho_M(r)$ is the proton's magnetization density, and $r = |\vec{r}|$ is the distance from the center of the proton.

The FAMU Collaboration [6–11] employs a method that exploits the energy dependence of muon transfer from hydrogen to heavier nuclei. A pulsed low-energy muon beam is stopped inside a cryogenic target containing an hydrogen-oxygen mixture. Muonic hydrogen is first formed in the H_2-O_2 gas mixture and then irradiated by a laser tuned near the hyperfine transition resonance at $\Delta E^{\mathrm{hfs}}_{1s}/h \approx 44\,\mathrm{THz}$ (see the top-left panel of figure 1). When μH is excited by the laser, collisions with oxygen are enhanced, leading to an excess of muon transfer reactions ($\mu p + \mathrm{O}_2 \rightarrow \mu\mathrm{O} + \mathrm{O} + \mathrm{p}$).

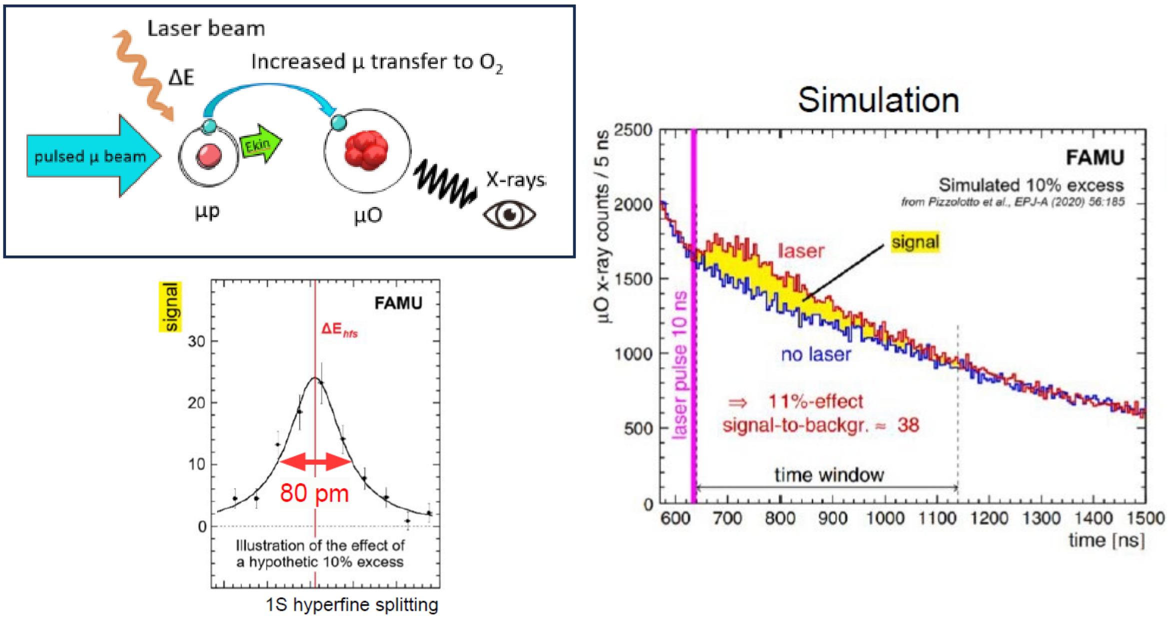

Figure 1. Schematic overview of the FAMU method. Reproduced from [11]. CC BY 4.0. Top-left panel: the $1S$ hyperfine transition in muonic hydrogen (μH) is driven by a mid-infrared (MIR) laser pulse. Excited atoms transfer the muon to oxygen molecules, and the transition is tagged by detecting the characteristic X-rays from muonic oxygen (μO) de-excitation. Right panel: simulated distribution of the FAMU observable with laser/no-laser irradiation. Bottom-left panel: expected 1S HFS resonance width.

The reaction is detected through characteristic X-rays emitted during the de-excitation of muonic oxygen. The resonance condition is identified by a distortion in the time distribution of muon transfer events compared to the laser-off condition, as shown in the right panel of figure 1. Laser-excited μH atoms gain about 0.12 eV of kinetic energy, which increases the muon transfer rate $\lambda_{pO}(E)$ to oxygen. Since $\lambda_{pO}(E)$ grows sharply with energy (at near-thermal energies) in an $H_2 - O_2$ mixture [12–14], this enhances the observable X-ray signal.

The key experimental challenge is the laser excitation of the ortho ($F = 1$) hyperfine state from the para ($F = 0$) state, where $F = F_p + F_\mu$ is the total spin of the μH atom. This magnetic dipole transition is extremely weak, with a transition probability: $P = 2 \times 10^{-5}\, (E[\mathrm{J}])\, (S[\mathrm{m}^2])^{-1}\, (T[\mathrm{K}])^{-1/2}$, where E is the laser pulse energy, S the laser beam cross section, and T the target temperature [4]. To reach a detectable signal, an optical multi-pass cavity (MOC) is used to enhance the interaction rate. To isolate the extremely weak hyperfine transition, high-resolution X-ray spectroscopy and stringent background suppression are also required.

2026 JINST 21 C01029

Several experimental programs are pursuing measurements related to the proton Zemach radius. One of the closest competitors is the CREMA Collaboration (Charge Radius Experiment with Muons) at PSI, which has already performed landmark measurements of the Lamb shift in muonic hydrogen and deuterium. CREMA has proposed a dedicated experiment to measure the $1S$ hyperfine splitting (HFS) in muonic hydrogen using Doppler-free two-photon laser spectroscopy [15], with the goal of extracting the Zemach radius from purely atomic physics observables, similarly to FAMU but employing a different method based on cascade X-ray detection.

An alternative experimental approach is under study at J-PARC, where high-intensity pulsed muon beams are proposed to study the HFS of muonic hydrogen using cryogenic hydrogen targets [16]. These efforts share FAMU's objective of improving the precision of the proton's electromagnetic structure parameters and aim to minimize systematic uncertainties associated with gas mixtures and collision dynamics.

In addition to these direct HFS measurements, constraints on the Zemach radius also arise from scattering experiments. The MUSE experiment at PSI uses simultaneous e-p and $\mu - p$ scattering to test lepton universality and to provide form factor data at very low momentum transfer [17]. While it does not measure the Zemach radius directly, MUSE helps to constrain theoretical inputs relevant to Zemach radius extraction. Similarly, high-precision electron scattering experiments such as the Mainz A1 program [18] and the PRad experiment at Jefferson Lab [19] provide crucial input for dispersion relation calculations of the Zemach radius from proton magnetic form factors.

2 The RIKEN-RAL muon complex

The ISIS 800 MeV/c primary proton beam, impinging on a secondary graphite target, produces pions decaying to muons. If the pion decay is inside the target, surface muons are produced with a momentum peaking around 29 MeV/c. If instead the pion decays outside the target, decay muons in the range 17–120 MeV/c are produced. The RIKEN-RAL muon complex [20] delivers secondary muon beams to four experimental ports, of which port 1 is presently used by the FAMU experiment. FAMU makes use of negative decay muons at ~ 55 MeV/c. With an intensity of $\sim 1.2 \times 10^5 \mu^- / s$ the beam has a momentum spread $\sigma_p / p = 4\%$ and an angular divergence ~ 60 mrad. The beam has a double pulse structure (70 ns FWHM widths, 320 ns peak to peak distance) reflecting the primary beam structure.

3 The FAMU experimental apparatus

The FAMU experimental apparatus is shown in the right panel of figure 2. Incoming muons at around 55 MeV/c impinge on a gaseous hydrogen target, inside a cryogenic vessel containing LN_2. A multipass optical cavity (MOC), inside the target, is used to increase the rate of muonic hydrogen interactions with photons from the mid-infrared (MIR) laser system. Surrounding the vessel three rings of $LaBr_3$:Ce detectors are used to detect signal X-rays, in addition to one HPGe utilized for precision cross-calibrations. The detectors in the upstream and downstream rings use a SiPM array readout, while in the central ring six detectors use a PMT readout [21] and the other six a SiPM array readout [22–24]. In 2023 data taking (configuration A), the downstream ring was equipped with cubic 1/2″ crystal detectors, read by Hamamatsu S14161-3050-AS4 SiPM arrays, while from 2024 (configuration B) these detectors were replaced by 1″ round, 1/2″ thick crystals read by S14161-6050-AS4 SiPM arrays, to increase solid angle coverage. In front of the cryogenic vessel entrance 0.2 mm aluminized Mylar window, a beam hodoscope with 64 channels in X/Y was placed to optimize the beam steering into the target and evaluate the muon beam intensity.

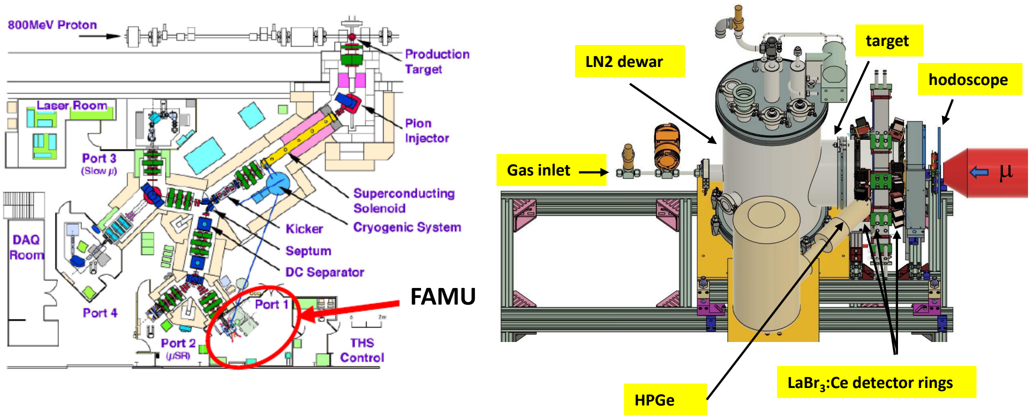

Figure 2. Left: layout of the RIKEN-RAL complex. Right: setup of the FAMU experiment at Port 1.

3.1 The FAMU beam hodoscope

The current FAMU beam hodoscope is the last of a series of devices [25, 26] that have demonstrated the soundness of the chosen approach. It is based on 32+32 1 mm^2 square Bicron BCF-12 scintillating fibers, coated with EMA to avoid light cross-talk, along X/Y directions, with a fiducial area of $64 \times 64\,\text{mm}^2$. Fibers, with a 1 mm spacing, are read at alternate ends by Hamamatsu S12751-50P SiPMs with 50 µm cells. The internal structure of the hodoscope is shown in figure 3. 16 SiPMs for each side are soldered on a PCB and have the same bias. Signals are then fanned out through MCX connectors to CAEN V1730 FADC. The main use of the beam hodoscope is to optimize the beam steering onto the target. In addition it may be used also to evaluate the impinging beam intensity, by measuring the charge deposited in the detector's fibers (Q_{TOT}) [27]. If Q_μ is the charge for a single muon, the incoming muon intensity may be estimated from: $\phi[\mu/s] = \kappa \times Q_{TOT}$, where κ is a function of Q_μ. After initial studies at INFN MIB laboratory to estimate κ with cosmic muons, a more accurate estimation was performed in reference [28] using data collected both at RAL and at the CNAO proton synchroton. Results on beam rate and profile are shown in figure 3.

3.2 The fast X-ray detection system

The main requirements for the FAMU X-ray detectors include: good energy resolution around 150 keV, for optimal detection of the K_α and $K_{\beta,\gamma}$ spectral lines from oxygen de-excitation signal; fast response: especially the falltime (less than 200–300 ns), for optimal separation of signal (delayed) from background (prompt) and good angular coverage, to increase statistics. This has lead to the choice of $LaBr_3$:Ce crystals with PMT or SiPM array readout. Their main performances are shown in table 1, using both data from laboratory tests (at 120 and 662 keV) and from ISIS beam (at 142 keV). The worse results at 142 keV at Port 1, with respect to 120 keV for the PMT readout, are due probably to ageing effects of the used crystals, as they were taken some years later.

The exploded view of a 1″ LaBr3:Ce detector with SiPM array readout is shown in figure 4. All X-rays detectors have been calibrated offline with Am^{241}, Ba^{133} and Cs^{137} sources before data taking. Remaining gain variation in %, along the October 2023 beamtime, for the central ring detectors

2026 JINST 21 C01029

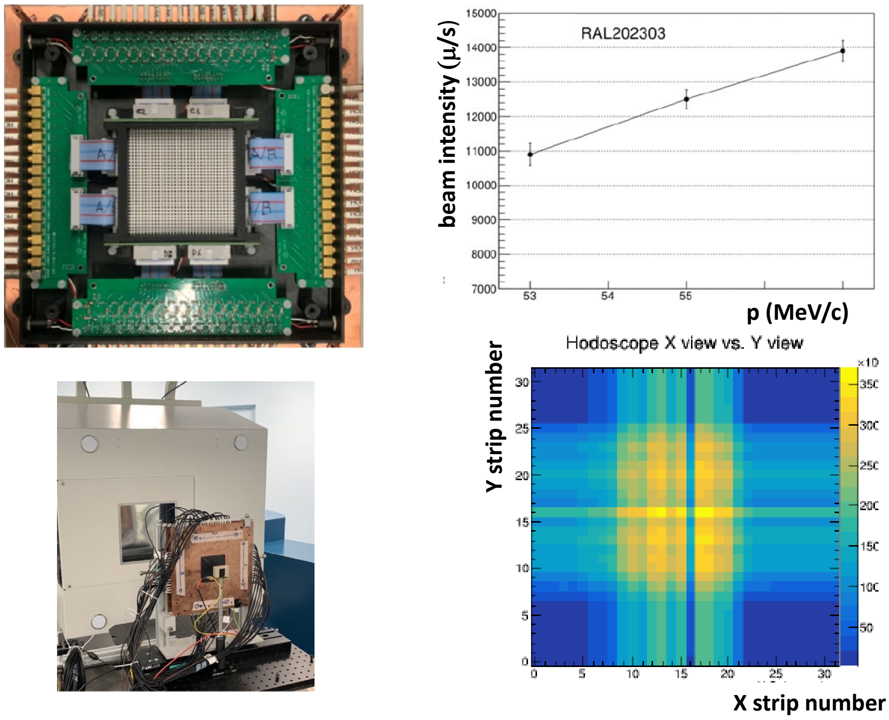

Figure 3. Left panel: top – inside view of the beam hodoscope; bottom – beam hodoscope photograph at CNAO. Right panel: top – muon beam rate vs muon momentum; bottom – X/Y beam profile. Reproduced from [28]. CC BY 4.0.

Table 1. Average performances of FAMU X-ray detectors. Rise time and fall time (10–90 %) in ns (at 662 keV) refer to detectors' summed analog outputs. FWHM energy resolutions (R) are in percent.

	1″ – PMT	1″ – SiPM	1/2″ – SiPM	HpGe
rise time (ns)	14 ± 1	29.3 ± 1.5	42.8 ± 4.7	150
fall time (ns)	∼ 60	147.1 ± 12.8	372.4 ± 17.4	1000–2000
R (%) @ 120 keV	7.2–8.1	8.03 ± 0.39	8.44 ± 0.63	1.010 ± .001
R (%) @142 keV	12.3 ± 1.2	7.0 ± 0.3	7.5 ± 0.3	1.26 ± 0.17
R (%) @662 keV	3.5–4.6	2.94 ± 0.14	3.27 ± 0.11	.442 ± .001

with SiPM array readout are shown in the bottom left panel of figure 4. An offline calibration is applied later to all detectors, using the peaks present in the data as shown in the top-right panel of the same figure. The detectors with SiPM readout have better FHWM energy resolution, than the ones with PMT readout,but at the cost of an increased falltime. 1/2″ detectors use a conventional parallel ganging. Falltime has been reduced by a factor 2X for 1″ detectors, by using an innovative 4-1 PCB developed in collaboration with Nuclear Instruments srl [29, 30]. As shown in [31], SiPM's gain drifts as a function of temperature. To correct online for this effect, a custom solution based on CAEN A7585 power modules, has been studied [32]. As the stability of the temperature in Port 1 is within ±1°C, this online correction has not been implemented up to now. Further details on the FAMU $LaBr_3$:Ce detectors' system are reported in reference [33].

2026 JINST 21 C01029

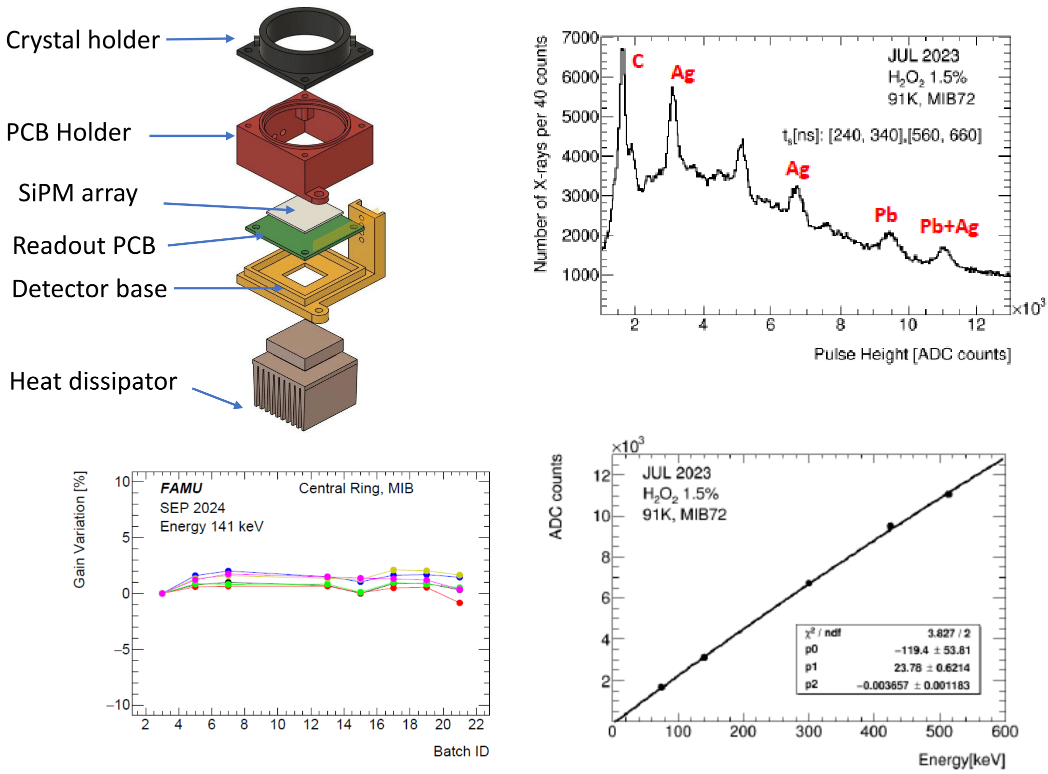

Figure 4. Top-left:exploded view of one 1″ $LaBr_3$:Ce detector with SiPM array readout. Bottom-left:gain variation along October 2023 data taking for the six central ring detectors, with SiPM array readout. Reproduced from [11]. CC BY 4.0. Batch ID refer to runs taken with different wavelength. Top-right: marked peaks are used for offline calibration for a SiPM readout detector. Bottom-right: obtained results of the offline calibration. Reproduced from [33]. CC BY 4.0.

3.3 The cryogenic target and multipass optical cavity

The FAMU cryogenic target, see figure 5, is made of an external vessel containing LN_2, as cooling liquid and an internal target containing the $H_2 + O_2$ (1.5 %) mixture, at 7 bar.[1]

Inside the internal target the MOC increases the probability of μH laser photon interactions by multiple reflection: $\sim 10^3$ from simulation. The MOC is made with two fused silica mirrors, coated with ZnS/Ge multilayers, with a 99.890(2) % reflectivity at 6.78 µm. Laser pulses are injected into the MOC by a flange connected to an external channel, where they are transmitted in a dry air atmosphere, to reduce MIR light absorption. This implies a complex alignment procedure. To simplify it, an injection system based on MIR optical fibers is under study at INFN MIB [34], for future upgrades.

3.4 The MIR laser system

Laser light at around 6800 nm is produced by a difference frequency generation (DFG) process inside a non linear $BaGa_4Se_7$ $10{\times}10{\times}27\,mm^3$ crystal. A tunable laser at $\lambda_1 = 1262$ nm, together with a fixed laser system at $\lambda_2 = 1064$ nm allows a final wavelength tuning around 6800 nm as deduced from: $\lambda_{DFG}^{-1} = \lambda_1^{-1} - \lambda_2^{-1}$.

[1]A static cooling method, based on a 5 liter LN2 reservoir, was chosen instead of cryocoolers, to avoid vibrations dangerous to the alignment of the laser system.

2026 JINST 21 C01029

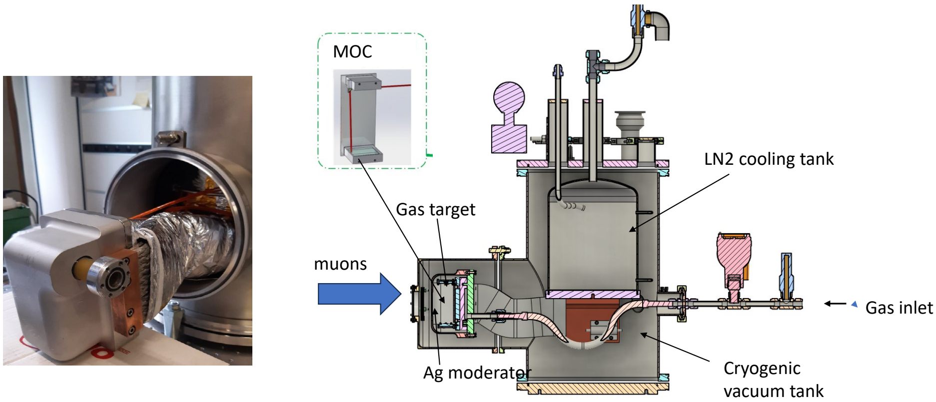

Figure 5. Left panel: picture of the inner target, containing the H_2-O_2 gas mixture. Right panel: layout of the FAMU target cryostat, with the main components. The inset shows the MOC. Reproduced from [6]. CC BY 4.0.

A schematic layout of the DFG laser system, used in FAMU, is shown in the top panel of figure 6. For further details see [35, 36]. A laser energy in excess of 1.5 mJ is currently obtained.

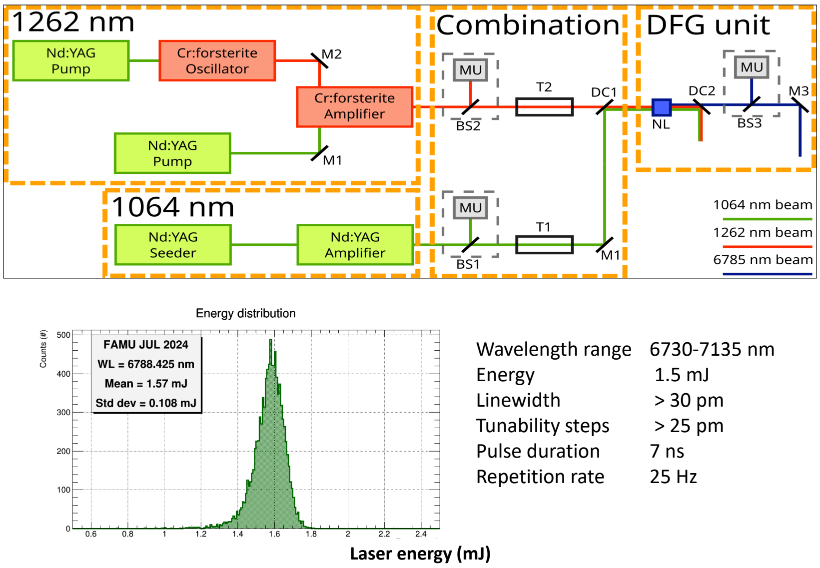

Figure 6. Top panel: schematic layout of the DFG laser system used in the FAMU experiment. Reproduced from [5]. CC BY 4.0. Bottom-left panel: laser energy distribution; bottom-right panel: laser characteristics.

4 FAMU data taking

After an extensive commissioning phase, where the feasibility of the method to measure the energy of the HFS 1S transition, via muon transfer from μH to Oxygen contaminants, was demonstrated [12–14] and both the laser [35, 36] and detectors [33] systems were developed, data taking for physics began in September 2023. The summary of the data acquisition periods is shown in table 2.

About 49 days of beam time were allocated in total, covering 26 wavelengths in the range 6788.425, 6789.050 nm with a 25 pm step between measurements. Two additional periods are foreseen for the last part of 2025.

Table 2. Summary of data taking periods in 2023–2024. (A) and (B) refer to setup described in section 3.

period	no. triggers	exp setup
October 2023	1.60×10^7	A
December 2023	2.65×10^7	A
July 2024	2.12×10^7	B
September 2024	2.15×10^7	B

5 FAMU data analysis: preliminaries

Data analysis is based on the observation of an excess in the number of delayed μO X-rays when laser pulses at a frequency $\nu = \nu_{\mathrm{HFS}}$ are injected in the target, with respect to no-laser events. By varying the laser frequency ν, a scan of the resonance curve is made. By using in sequence a trigger with laser injection and one without a laser injection in coincidence with the arrival of the ISIS beam, systematics may be reduced, as compared to other experiments. As a first point, a good X-ray detectors' response is needed to show the signal K_α and $K_{\beta,\gamma}$ Oxygen lines, as shown in the top panel of figure 7. Further effects, to be taken into account, are: normalization to beam intensity fluctuations, as measured by the beam hodoscope, target conditions (T,p), laser conditions, in terms of wavelength and energy stability, time alignment of X-ray detectors' response with respect to the laser shot. A preliminary consistency test for the analysis is based on the request to obtain a zero

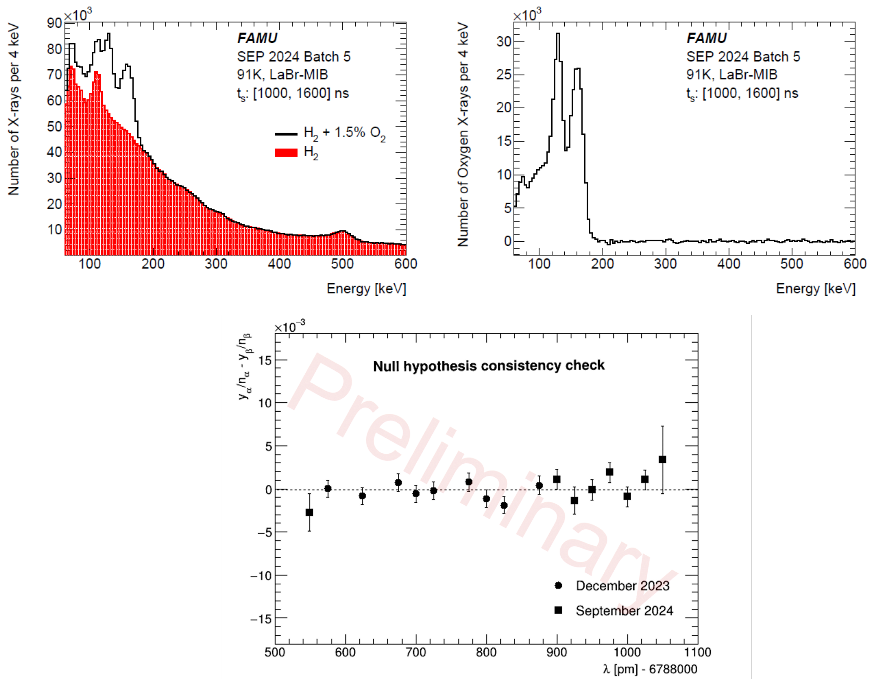

Figure 7. Top panel: delayed spectrum (time bin [1000,1600] ns) for all $LaBr_3$:Ce detectors in batch 5 of October 2024 run; right: same with subtraction of the H_2 background. Reproduced from [11]. CC BY 4.0. K_α, $K_{\beta/\gamma}$ signal lines are evident. Events under the two peaks are due to imperfect containment inside the crystals. Bottom panel: difference of sample α /sample β number of events with a random tagging. y is the number of collected X-rays, while n is the number of acquired triggers for the two samples.

2026 JINST 21 C01029

signal, by a random tagging of events in two samples called sample α and sample β, without taking into account if the laser pulse was effectively injected or not. The result of this consistency test is shown for the 2023–2024 data in the bottom panel of figure 7.

6 Conclusions and perspectives

The FAMU experiment, after nearly a decade of tests to validate the detection method proposed, has been installed in its final configuration at RAL in 2023. Four successful physics runs have been performed in 2023 and 2024 and has been followed by two other data taking periods in 2025. Its two main components: the high-performance X-ray detectors system and the high-energy MIR laser have shown good performances. The results of the data analysis are expected soon.

Acknowledgments

We would like to thank A. Abba and F. Capogno of Nuclear Instruments and M. Saviozzi of CAEN for many enlightning discussions on electronics items and SiPM readout.

References

[1] A. Antognini, F. Hagelstein and V. Pascalutsa, *The proton structure in and out of muonic hydrogen*, *Ann. Rev. Nucl. Part. Sci.* **72** (2022) 389 [arXiv:2205.10076].

[2] R. Pohl et al., *The size of the proton*, *Nature* **466** (2010) 213.

[3] A. Antognini et al., *Proton Structure from the Measurement of* 2*S*-2*P* *Transition Frequencies of Muonic Hydrogen*, *Science* **339** (2013) 417.

[4] A. Adamczak, D. Bakalov, L. Stoychev and A. Vacchi, *Hyperfine spectroscopy of muonic hydrogen and the PSI Lamb shift experiment*, *Nucl. Instrum. Meth. B* **281** (2012) 72.

[5] A.C. Zemach, *Proton Structure and the Hyperfine Shift in Hydrogen*, *Phys. Rev.* **104** (1956) 1771.

[6] A. Vacchi et al., *Measuring the size of the proton*, *SPIE Newsroom* (2012).

[7] A. Adamczak et al., *The FAMU experiment at RIKEN-RAL to study the muon transfer rate from hydrogen to other gases*, 2018 *JINST* **13** P12033.

[8] M. Bonesini, *The FAMU experiment at RIKEN RAL for a precise measure of the proton radius*, arXiv:2010.01398.

[9] C. Pizzolotto et al., *The FAMU experiment: muonic hydrogen high precision spectroscopy studies*, *Eur. Phys. J. A* **56** (2020) 185.

[10] A. Vacchi et al., *Investigating the Proton Structure: The FAMU Experiment*, *Nucl. Phys. News* **33** (2023) 4 [arXiv:2403.05145].

[11] A. Adamczak et al., *First operation of the FAMU experiment at the RIKEN-RAL high intensity muon beam facility*, *Eur. Phys. J. A* **61** (2025) 284 [arXiv:2509.10350].

[12] E. Mocchiutti et al., *First measurement of the temperature dependence of muon transfer rate from muonic hydrogen atoms to oxygen*, *Phys. Lett. A* **384** (2020) 126667 [arXiv:1905.02049].

[13] M. Stoilov et al., *Experimental determination of the energy dependence of the rate of the muon transfer reaction from muonic hydrogen to oxygen for collision energies up to 0.1 eV*, *Phys. Rev. A* **107** (2023) 032823 [arXiv:2303.15575].

[14] C. Pizzolotto et al., *Measurement of the muon transfer rate from muonic hydrogen to oxygen in the range 70–336 K*, *Phys. Lett. A* **403** (2021) 127401 [arXiv:2105.06701].

[15] P. Amaro et al., *Laser excitation of the 1s-hyperfine transition in muonic hydrogen*, *SciPost Phys.* **13** (2022) 020 [arXiv:2112.00138].

[16] S. Kanda et al., *Measurement of the proton Zemach radius from the hyperfine splitting in muonic hydrogen atom*, *J. Phys. Conf. Ser.* **1138** (2018) 012009.

[17] S. Strauch, *The MUon Scattering Experiment (MUSE) at the Paul Scherrer Institute*, *PoS* **CD2021** (2024) 070.

[18] I. Sick, *Problems with proton radii*, *Prog. Part. Nucl. Phys.* **67** (2012) 473.

[19] W. Xiong et al., *A small proton charge radius from an electron-proton scattering experiment*, *Nature* **575** (2019) 147.

[20] T. Matsuzaki et al., *The RIKEN-RAL pulsed muon facility*, *Nucl. Instrum. Meth. A* **465** (2001) 365.

[21] G. Baldazzi et al., *The $LaBr_3$(Ce) based detection system for the FAMU experiment*, 2017 *JINST* **12** C03067.

[22] M. Bonesini et al., *Detection of low-energy X-rays with 1/2 and 1 inch LaBr3:Ce crystals read by SIPM arrays*, *PoS* **EPS-HEP2021** (2022) 770 [arXiv:2202.08746].

[23] M. Bonesini et al., *Ce:$LaBr_3$ crystals with SiPM array readout and temperature control for the FAMU experiment at RAL*, 2020 *JINST* **15** C05065 [arXiv:2003.08971].

[24] M. Bonesini et al., *One inch LaBr3:Ce detectors, with temperature control and improved time resolution for low energy X-rays spectroscopy*, *PoS* **EPS-HEP2023** (2024) 547 [arXiv:2312.08547].

[25] R. Carbone et al., *The fiber-SiPMT beam monitor of the R484 experiment at the RIKEN-RAL muon facility*, 2015 *JINST* **10** C03007.

[26] M. Bonesini et al., *The construction of the Fiber-SiPM beam monitor system of the R484 and R582 experiments at the RIKEN-RAL muon facility*, 2017 *JINST* **12** C03035 [arXiv:1703.01447].

[27] M. Bonesini et al., *The upgraded beam monitor system of the FAMU experiment at RIKEN-RAL*, *Nucl. Instrum. Meth. A* **936** (2019) 592.

[28] R. Rossini et al., *The muon beam monitor for the FAMU experiment: design, simulation, test, and operation*, *Front. Detect. Sci. Tech.* **2** (2024) 1438902 [arXiv:2410.07257].

[29] M. Bonesini et al., *Large area LaBr3:Ce crystals read by SiPM arrays with improved timing and temperature gain drift control*, *Nucl. Instrum. Meth. A* **1046** (2023) 167677 [arXiv:2211.05081].

[30] M. Bonesini et al., *Improving the Time Resolution of Large-Area $LaBr_3$:Ce Detectors with SiPM Array Readout*, *Condens. Mat.* **8** (2023) 99 [arXiv:2311.15949].

[31] A. Nepomuk Otte, D. Garcia, T. Nguyen and D. Purushotham, *Characterization of Three High Efficiency and Blue Sensitive Silicon Photomultipliers*, *Nucl. Instrum. Meth. A* **846** (2017) 106 [arXiv:1606.05186].

[32] M. Bonesini, R. Bertoni, M. Prata and M. Rossella, *Online control of the gain drift with temperature of SiPM arrays used for the readout of $LaBr_3$:Ce crystals*, 2022 *JINST* **17** C10004 [arXiv:2210.02258].

[33] M. Bonesini, *The fast X-ray detector system of the FAMU experiment at RAL*, *Nucl. Instrum. Meth. A* **1080** (2025) 170780 [arXiv:2507.01819].

[34] R. Benocci et al., *Laboratory tests for MIR light detection and transport with specialty optical fibres*, 2020 *JINST* **15** C04030 [arXiv:2004.01414].

[35] M. Baruzzo et al., *A mid-IR laser source for muonic hydrogen spectroscopy: The FAMU laser system*, *Opt. Laser Tech.* **179** (2024) 111375.

[36] M. Baruzzo et al., *Long-Term performance of a Mid-IR Laser system for Muonic Hydrogen Spectroscopy: Insights from the FAMU Experiment*, DOI:10.2139/ssrn.5464154.

2026 JINST 21 C01029